RSC Advances

PAPER

View Article Online
View Journal | View Issue

Cite this: *RSC Adv.*, 2019, **9**, 17852

A promising Mo-based lithium-rich phase for Li-ion batteries

Yongqing Wang, [a] Haoshen Zhou *[bc] and Hongbing Ji *[a]

Received 8th May 2019
Accepted 26th May 2019

DOI: 10.1039/c9ra03449h

rsc.li/rsc-advances

Herein, we demonstrate a composite Mo-based lithium-rich $Li_2MoO_4 \cdot LiNi_{0.4}Mn_{0.4}Co_{0.2}O_2$ material, which exhibits a higher practical capacity of 270 mA h g^{-1}, and better capacity retention (61% after 50 cycles) when compared with the well-known Li_2MnO_3.

There is growing interest in developing high capacity electrode materials for lithium ion batteries.[1,2] The strategy of using a lithium rich component, *e.g.* Li_2MnO_3, to enhance the electrochemical capacity of layered $LiMO_2$ (M = a transition metal element or its mixture) has been intensively studied since 2000.[3–6] However, Li_2MnO_3 suffers from severe capacity and voltage fading during cycling.[7,8–14] Although surface modification[15] and elemental substitution[16–18] have been used to improve the electrochemical stability, its inherent shortcomings have not been fundamentally resolved. A search for alternatives is thus greatly required for high-capacity lithium ion batteries.[19–23]

Previous theoretical[23,24] and experimental studies[25–27] have shown that Li_2MoO_3 has higher electronic conductivity and better stability than Li_2MnO_3, because of the coexistence of Mo^{6+}/Mo^{5+} valence states during lithium insertion/extraction. However, directly obtaining Li_2MoO_3–$LiMO_2$ composites through high-temperature solid-state reaction (SSR) poses a substantial challenge, because Mo^{6+} is more stable at high temperature. Thus, we suggest Li_2MoO_4 as a lithium rich phase and fabricate a Li_2MoO_4–$LiNi_{0.4}Mn_{0.4}Co_{0.2}O_2$ material (denoted as LMLNMC) directly through high-temperature SSR. A coin-type lithium half-cell with LMLNMC as the cathode exhibits a specific capacity of 270 mA h g^{-1} in the voltage range of 1.0–4.8 V, which is comparable to that of the Li_2MnO_3-based composite. Additionally, we found an interesting structure change from Li_2MoO_4 toward Li_3MoO_4 at *ca.* 1.0 V during lithium insertion.[28] These findings provide a new platform for future high capacity electrode materials.

Fig. 1a shows the XRD pattern of the LMLNMC material. The majority of the X-ray diffraction peaks can be attributed to rhombohedral Li_2MoO_4 (JCPDS card no. 12-0768, space group $R\bar{3}$, $a = 14.34$ Å, $c = 9.59$ Å). The characteristic (003) diffraction peak of typical $LiMO_2$ layered structures could also be observed, which indicates the presence of $LiNi_{0.4}Mn_{0.4}Co_{0.2}O_2$ (red dashed arrows). Fig. 1b and c show the typical scanning electron microscopy (SEM) and transmission electron microscopy (TEM) images of the LMLNMCO after calcination. Both images show that the sample consists of nanoparticles with an average

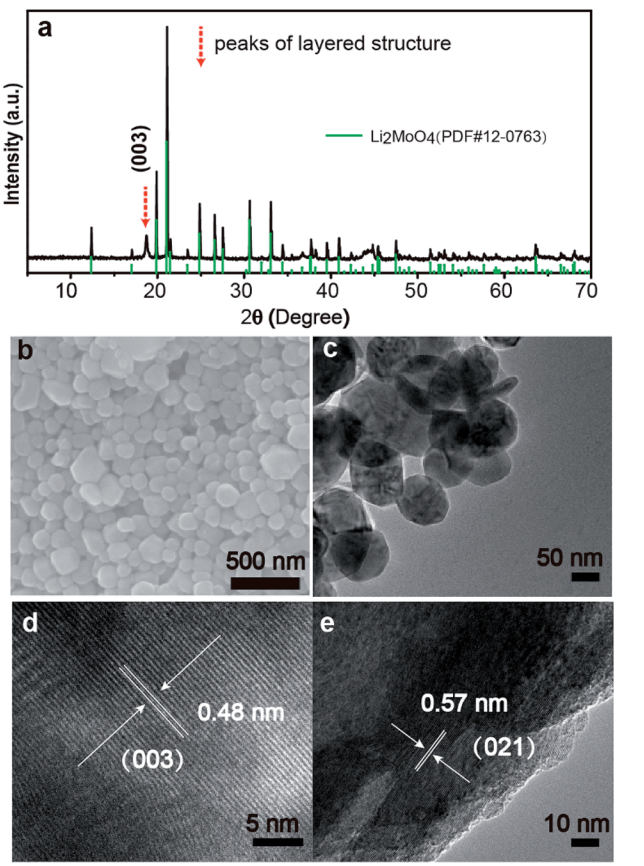

Fig. 1 Morphological and structural characteristics of LMLNMC. (a) The XRD pattern; (b) SEM and (c) TEM images; (d) and (e) HRTEM images.

[a]*Fine Chemical Industry Research Institute, School of Chemistry, Sun Yat-Sen University, Guangzhou 510275, P. R. China. E-mail: jihb@mail.sysu.edu.cn*

[b]*College of Engineering and Applied Sciences, Nanjing University, 210093, P. R. China*

[c]*National Institute of Advanced Industrial Science and Technology (AIST), Umezono 1-1-1, Tsukuba, 305-8568, Japan*

diameter of 100–200 nm. The smooth morphology also suggests that the composite forms a homogenous mixture during solid-state reaction. Fig. 1d and e show that the *d*-spacings from the HRTEM images are 0.48 nm and 0.57 nm, which can be well indexed with the (003) facets from the layered structure of $LiNi_{0.4}Mn_{0.4}Co_{0.2}O_2$ and (021) facets of rhombohedral Li_2MoO_4, respectively.

To address the electrochemical performance of LMLNMC, we investigated the charge and discharge profiles toward Li insertion/extraction. Coin-type cells with LMLNMCO as the cathode and Li metal as the anode were studied at a current density of 10 mA g^{-1} in the voltage range of 1.0–4.8 V (*vs.* Li^+/Li). Fig. 2a and b show the charge/discharge profiles. In the first charge process, the composite LMLNMCO material shows a specific capacity of *ca.* 78 mA h g^{-1} from 3.0 to 4.5 V, which mainly corresponds to the contribution from $LiNi_{0.4}Mn_{0.4}Co_{0.2}O_2$. Meanwhile, during the first discharge process, in addition to the contribution from $LiNi_{0.4}Mn_{0.4}Co_{0.2}O_2$ (*ca.* 30 mA h g^{-1}) from 4.5 V to 3.0 V, a long discharge plateau appeared at *ca.* 1.0 V (*ca.* 235 mA h g^{-1}), which can be attributed to lithium insertion into Li_2MoO_4. However, in the following cycles, an obvious voltage slope appeared between 1.5 and 2.5 V, distinct from the first cycle, which probably implies that a structural change of Li_2MoO_4 appeared during the first lithium insertion process. The battery was also cycled at a current density of 10 mA g^{-1} in the voltage range of 1.0–4.8 V (*vs.* Li^+/Li), and showed a capacity retention of about 61% after 50 cycles. The rate performance of this material was tested at 20 mA g^{-1} in the same voltage range, and compared with the results at 10 mA g^{-1}, the charge and discharge capacity of this material decreased quickly from *ca.* 250 mA h g^{-1} to *ca.* 80 mA h g^{-1}. This poor rate capability is similar to that observed for its Li_2MnO_3 analog, and still needs ongoing improvement for future applications.

An *ex situ* X-ray diffraction experiment was carried out on commercial Li_2MoO_4 material and LMLNMCO to provide a general overview of the structure evolution of Li_2MoO_4 before and after lithium insertion. Fig. 3 shows the X-ray diffraction patterns. Commercial Li_2MoO_4 before lithium insertion shows a similar rhombohedral phase to LMLNMCO. However, an apparent structure change can be observed after lithium insertion. Two phases could be observed in Fig. 3. (1) An Li_3MoO_4 phase with a space group of $Fm\bar{3}m$, similar to that of rocksalt-like NaCl structures, marked with dashed red arrows (Fig. 3, top); the peaks could be well indexed as (111), (200), and (220) of Li_3MoO_4, respectively. (2) Rhombohedral $Li_{2+x}MoO_4$, similar to Li_2MoO_4, but with a larger lattice.[27] Scheme 1 illustrates the crystal structure change from Li_2MoO_4 to Li_3MoO_4 during lithium insertion, suggesting a structure change to a rock-salt structure, which is more similar to a layered structure and means that the structures are more likely to merge with each other. This structure change implies the instability of Li_2MoO_4 toward lithium insertion, but it provides the possibility of using an *in situ* electrochemical synthesis process to produce Mo^{4+}-based lithium-rich composite electrode materials for future high-capacity lithium ion batteries.

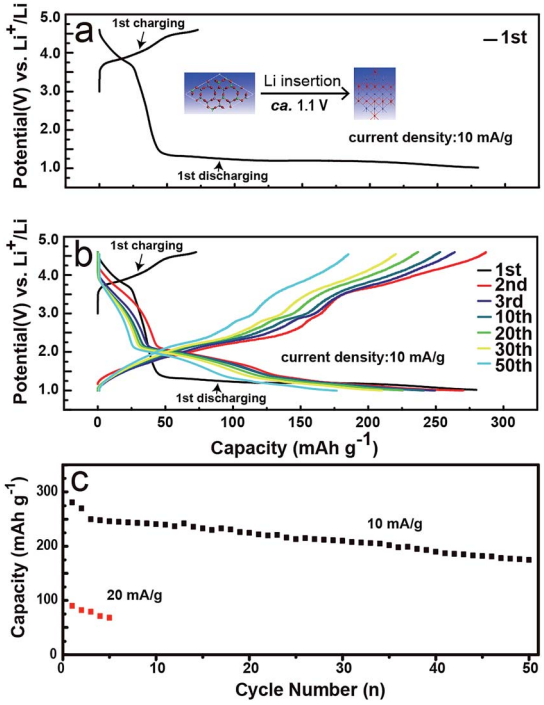

Fig. 2 Electrochemical characterization of LMLNMCO. (a) and (b) Galvanostatic charge and discharge profiles; (c) cycle performance.

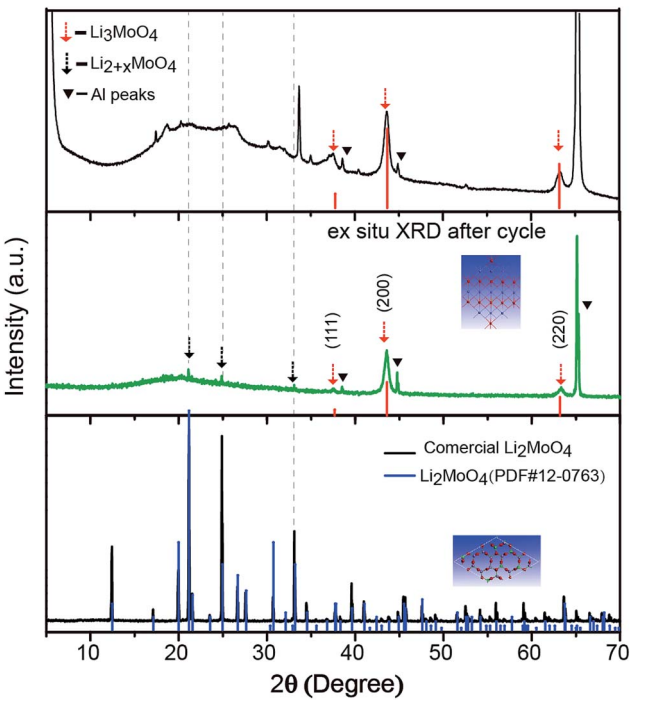

Fig. 3 The X-ray diffraction pattern of commercial Li_2MoO_4 (bottom), and the *ex situ* diffraction pattern of commercial Li_2MoO_4 (middle) and LMLNMCO (top) after 10 cycles when used as a cathode for lithium half cells.

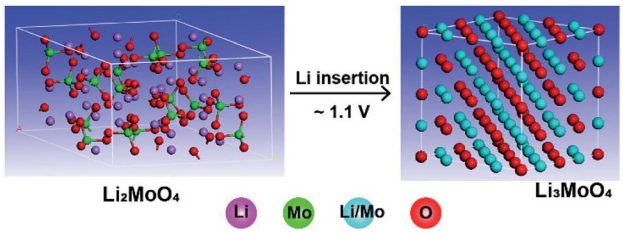

Scheme 1 The crystal structure change from Li_2MoO_4 to Li_3MoO_4 during lithium insertion.

Conclusions

In conclusion, a lithium-rich $Li_2MoO_4 \cdot LiNi_{0.4}Mn_{0.4}Co_{0.2}O_2$ composite material was obtained directly from high temperature solid-state reactions under an air atmosphere at 700 °C for 10 h. Li_3MoO_4 has a much higher lithium content than Li_2MoO_3 and the Mo^{4+}/Mo^{6+} redox couple can exchange multiple electrons and provide more specific capacity. The material shows a high specific capacity and exhibits a high initial coulombic efficiency in our study. Additionally, we found that Li_2MoO_4 undergoes a phase change toward Li_3MoO_4 after lithium insertion at *ca.* 1.0 V. With this phase change, the Mo^{4+}-based composite material is likely to be fabricated through an *in situ* electrochemical lithium insertion process. These advantages suggest that Li_2MoO_4 is a potential alternative for Li_2MnO_3. However, the cycling stability and rate performance of this material still need to be improved for future applications. The strategy here is simple yet very effective, and it may also be extended to other electrode materials for future high capacity Li-ion batteries used in electric vehicles and energy storage stations.

Methods

Material synthesis

The Mo-based LMLNMC material was synthesized by a high-temperature solid-state reaction. Stoichiometric amounts of Li_2MoO_4, $MnAc_2 \cdot 4H_2O$, $NiAc_2 \cdot 4H_2O$, $CoAc_2 \cdot 4H_2O$ and $LiOH \cdot H_2O$ were mixed together, ground in an agate mortar and then pressed into pellets. Each pellet was about 0.5 g, and the pellet was then heated in a muffle furnace at 700 °C for 10 h. The resulting material was stored in a glovebox under argon atmosphere to prevent reaction with moisture in the air. All the reactants were used as purchased.

Electrochemical tests

Electrochemical tests were carried out in 2032 coin-type cells with an arrangement of $Li|LiPF_6$ in EC : EMC : DEC (1 : 1 : 1, wt%)|LMO-LNMCO. The cells were assembled in an argon-filled glove box. To prepare the working electrode, LMO-LNMCO, Super-P, and PVDF (polyvinyl difluoride) were mixed at a weight ratio of 80 : 10 : 10 and ground in an agate mortar with a small volume of NMP (*N*-methyl-2-pyrrolidinone), and the obtained electrode slurry was then pasted on aluminum foil and dried in a vacuum oven at 100 °C after NMP was evaporated. The loading mass of active materials is about 2.5 mg cm^{-2}. Pure lithium foil was used as a counter electrode. Celgard-2400 film was used as a separator. Galvanostatic charge and discharge tests were undertaken in the voltage range of 1.0–4.8 V (*vs.* Li^+/Li) at a constant current density of 10 mA g^{-1}. The specific capacities were calculated based on the mass of active materials.

Structural characterization

The phase and crystallographic structure were characterized by powder X-ray diffraction (XRD) using a Bruker D8 Advanced diffractometer equipped with a Cu Kα1 (λ = 1.54056 Å) radiation source. An *ex situ* XRD method was used to characterize the structural evolution of Li_2MoO_4 and LMLNMCO after the electrochemical tests. The electrode foils after the test were removed from the coin-type cell, and washed with DMC solvent several times before being sealed on the sample stage for the XRD tests with Kapton film. All operations were carried out inside an argon-filled glove box to avoid side reactions with moisture in the air. The size and morphology of the samples were characterized using a JSM-6330F scanning electron microscope (SEM) operated at 10 kV. Transmission electron microscopy (TEM) and high-resolution TEM (HRTEM) microscopy were performed using a JEOL 2100F transmission electron microscope operated at an accelerating voltage of 200 kV.

Conflicts of interest

There are no conflicts to declare.

Acknowledgements

This work was financially supported by the National Natural Science Foundation of China (No. 21425627), the NFSC-SINOPEC Joint fund (No. U1663220), and the Natural Science Foundation of Guangdong Province (No. 2014A030308012).

References

1 M. S. Whittingham, *Chem. Rev.*, 2014, **114**, 11414–11443.
2 Y.-G. Guo, J.-S. Hu and L.-J. Wan, *Adv. Mater.*, 2008, **20**, 2878–2887.
3 K. Luo, M. R. Roberts, N. Guerrini, N. Tapia-Ruiz, R. Hao, F. Massel, D. M. Pickup, S. Ramos, Y.-S. Liu, J. Guo, A. V. Chadwick, L. C. Duda and P. G. Bruce, *J. Am. Chem. Soc.*, 2016, **138**, 11211–11218.
4 B. R. Long, J. R. Croy, J. S. Park, J. G. Wen, D. J. Miller and M. M. Thackeray, *J. Electrochem. Soc.*, 2014, **161**, A2160–A2167.
5 J. Bareño, C. H. Lei, J. G. Wen, S. H. Kang, I. Petrov and D. P. Abraham, *Adv. Mater.*, 2010, **22**, 1122–1127.
6 M. Sathiya, G. Rousse, K. Ramesha, C. P. Laisa, H. Vezin, M. T. Sougrati, M. L. Doublet, D. Foix, D. Gonbeau, W. Walker, A. S. Prakash, M. Ben Hassine, L. Dupont and J. M. Tarascon, *Nat. Mater.*, 2013, **12**, 827–835.

7 M. M. Thackeray, C. S. Johnson, J. T. Vaughey, N. Li and S. A. Hackney, *J. Mater. Chem.*, 2005, **15**, 2257–2267.
8 J. R. Croy, K. G. Gallagher, M. Balasubramanian, B. R. Long and M. M. Thackeray, *J. Electrochem. Soc.*, 2014, **161**, 9.
9 J. Liu, J. Liu, R. Wang and Y. Xia, *J. Electrochem. Soc.*, 2014, **161**, A160–A167.
10 Y. Li, J. Bareno, M. Bettge and D. P. Abraham, *J. Electrochem. Soc.*, 2015, **162**, A155–A161.
11 L. Li, R. Jacobs, P. Gao, L. Gan, F. Wang, D. Morgan and S. Jin, *J. Am. Chem. Soc.*, 2016, **138**, 2838–2848.
12 Y. Koyama, I. Tanaka, M. Nagao and R. Kanno, *J. Power Sources*, 2009, **189**, 798–801.
13 R. Xiao, H. Li and L. Chen, *Chem. Mater.*, 2012, **24**, 4242–4251.
14 S. Hy, F. Felix, J. Rick, W.-N. Su and B. J. Hwang, *J. Am. Chem. Soc.*, 2014, **136**, 999–1007.
15 F. Zheng, C. Yang, X. Xiong, J. Xiong, R. Hu, Y. Chen and M. Liu, *Angew. Chem., Int. Ed.*, 2015, **54**, 13058–13062.
16 J. Ma, Y.-N. Zhou, Y. Gao, Q. Kong, Z. Wang, X.-Q. Yang and L. Chen, *Chem.–Eur. J.*, 2014, **20**, 8723–8730.
17 Y. Gao, X. Wang, J. Ma, Z. Wang and L. Chen, *Chem. Mater.*, 2015, **27**, 3456–3461.
18 Y. Q. Wang, Z. Z. Yang, Y. M. Qian, L. Gu and H. S. Zhou, *Adv. Mater.*, 2015, **27**, 3915–3920.
19 X. Liu, Y. Lyu, Z. Zhang, H. Li, Y.-s. Hu, Z. Wang, Y. Zhao, Q. Kuang, Y. Dong, Z. Liang, Q. Fan and L. Chen, *Nanoscale*, 2014, **6**, 13660–13667.
20 K. S. Park, D. Im, A. Benayad, A. Dylla, K. J. Stevenson and J. B. Goodenough, *Chem. Mater.*, 2012, **24**, 2673–2683.
21 M. Zhang, G. Hu, L. Liang, Z. Peng, K. Du and Y. Cao, *J. Alloys Compd.*, 2016, **673**, 237–248.
22 D. Mikhailova, A. Sarapulova, A. Voss, A. Thomas, S. Oswald, W. Gruner, D. M. Trots, N. N. Bramnik and H. Ehrenberg, *Chem. Mater.*, 2010, **22**, 3165–3173.
23 J. Ma, Y. N. Zhou, Y. R. Gao, X. Q. Yu, Q. Y. Kong, L. Gu, Z. X. Wang, X. Q. Yang and L. Q. Chen, *Chem. Mater.*, 2014, **26**, 3256–3262.
24 M. Tian, Y. Gao, R. Xiao, Z. Wang and L. Chen, *Phys. Chem. Chem. Phys.*, 2017, **19**, 17538–17543.
25 D. Li, H. He, X. Wu and M. Li, *J. Alloys Compd.*, 2016, **682**, 759–765.
26 J. Ma, Y. Gao, Z. Wang and L. Chen, *J. Power Sources*, 2014, **258**, 314–320.
27 D. Li, H. Y. He, X. M. Wu and M. Q. Li, *J. Alloys Compd.*, 2016, **682**, 759–765.
28 D. Mikhailova, A. Voss, S. Oswald, A. A. Tsirlin, M. Schmidt, A. Senyshyn, J. Eckert and H. Ehrenberg, *Chem. Mater.*, 2015, **27**, 4485–4492.